Study on the photocatalysis of F–S co-doped TiO$_2$ prepared using solvothermal method

Guidong Yang [a,b], Zheng Jiang [b], Huahong Shi [b], Martin O. Jones [b,c], Tiancun Xiao [b,*],
Peter P. Edwards [b], Zifeng Yan [a,**]

[a] State Key Laboratory for Heavy Oil Processing, China University of Petroleum, Qingdao 266555, China
[b] Department of Chemistry, Inorganic Chemistry Laboratory, University of Oxford, South Parks Road, Oxford OX1 3QR, UK
[c] ISIS, STFC, RAL, Harwell Science and Innovation Campus, Didcot OX11 0QX, UK

ARTICLE INFO

ABSTRACT

Fluorine–sulfur (F–S) co-doped TiO$_2$ materials have been prepared using low-temperature solvothermal method, and tested for catalytic activity by the visible light photocatalytic degradation of the Methylene Blue. For comparison, the mono-elemental doped samples, e.g., S- and F-doped TiO$_2$ have also been prepared and tested under the same conditions. The characterization results showed that F–S co-doped TiO$_2$ has a higher photocatalytic activity than that of mono-doped F- and S-doped samples under visible light irradiation. It is believed that the co-doping gives rise to a localized state in the band gap of the oxide and creates active surface oxygen vacancies, both which are responsible for visible light absorption and the promotion of electrons from the localized states to the conduction band. Characterization by electron paramagnetic resonance revealed the presence of a superoxide radical ($O_2^{\bullet-}$) which may be mainly responsible for photodegradation of Methylene Blue under visible light.

© 2010 Elsevier B.V. All rights reserved.

1. Introduction

Titanium dioxide (TiO$_2$) is a well-known semiconductor photocatalyst that has attracted increasing attention due to its stability and low cost. Currently, its applications include the use of TiO$_2$-based nanomaterials in solar cells [1,2], highly efficient photocatalysts for decomposing organic compounds, water or air purification [3–5] and the generation of hydrogen by water splitting [6–8] under ultraviolet (UV) light (wavelength $\lambda < 388$ nm) illumination. The latter, in particular, is considered as a promising technology to address environmental problems and the global energy supply issue [9,10]. However, a major barrier to the widespread use of TiO$_2$ as photocatalysts is its relatively large electronic band gap, some 3.0–3.2 eV, limiting its photoresponse to visible light, which comprised of about 43% of the incoming solar energy. In order to extend the photoresponse of TiO$_2$ into the visible region of the solar spectrum, considerable efforts have been directed towards the doping of TiO$_2$ lattice to modify its electronic band gap and shift its absorption edge to the visible light region. One way this may be achieved is to dope TiO$_2$ with either nonmetal (or anion) or metal (or cations). For example, nonmetal (or anion) doping of TiO$_2$ by N [4], B [5,7], C [11] has shown a significant improvement of visible light-active TiO$_2$. Such nonmetal incorporation has been found to be able to enhance the optical adsorption in the visible region although this alone does not guarantee photocatalytic activity.

Recently, the possibility of such band gap engineering by the simultaneous incorporation of two nonmetal dopants – co-doping – has received much more attention [12–17]. Several authors have demonstrated the photocatalytic activity of nonmetal co-doping of TiO$_2$ for the photodegradation of organic pollutants, such as Methylene Blue, acetone and phenol in the visible part of solar spectrum. Chen et al. [14] found that co-doped TiO$_2$ nanotubes synthesized by the electrochemical anodization process, exhibit strong absorption in the visible light region, although co-doping does not result in significant improvement of photocatalytic activity under illumination of solar light (the photoelectrocatalytic efficiency of 4-CP over co-doping catalyst was 39.7%, and over mono-doping was 45%). Rengifo-Herrera et al. [15] used commercial TiO$_2$ nanopowder mechanically mixed with thiourea to prepare N and S co-doped TiO$_2$. The obtained material shows distinct photocatalytic activity when exposed to the visible light: DCA was not degraded, phe-

nol only partially decayed, while *E. coli* suffered fast inactivation. Xu et al. [16] reported that the co-doped photocatalyst prepared using a hydrolysis approach showed excellent photocatalytic activity for the decomposition of phenol under visible light due to the synergetic effects for its high surface area, large pore volume, well-crystallized anatase structure, red shift in absorption edge and strong absorbance of light with longer wavelength. Based on these previous studies, we have deduced that the nature of the synthesis methods exerts a significant effect on the photocatalytic properties of doped TiO$_2$ materials.

In the present work, a facile low-temperature solvothermal method has been developed to produce F–S co-doped TiO$_2$ of highly crystalline anatase phase, which is considered to be essential for photoactive catalysis. This synthesis method is not only energy efficient, but also environmentally conscious, as it avoids the use of any toxic precursors. The prepared TiO$_2$ materials are characterized by X-ray diffraction (XRD), X-ray photoelectron spectroscopy (XPS), Raman spectroscopy, Fourier transform infra-red (FT-IR), Electron paramagnetic resonance (EPR) and UV–vis DRS spectrophotometer. The photocatalytic activity of the nonmetal doped TiO$_2$ photocatalyst was evaluated using the decomposition of Methylene Blue (MB) solution as a model reaction and the visible light responsive mechanism of fluorine–sulfur (F–S) co-doped TiO$_2$ photocatalyst discussed.

2. Experimental

2.1. Synthesis of catalyst

The doped TiO$_2$ was prepared using a low-temperature solvothermal method, which is thought to give a uniform doping from the surface to the bulk of the materials. In a typical synthesis procedure, ammonia fluoride (NH$_4$F, 0.015 mol) and thiourea (CH$_4$N$_2$S, 0.015 mol) were dissolved in ethanol (C$_2$H$_5$OH, 30 ml) to give a solution which was then vigorously stirred for 30 min to generate a suspension. Tetrabutyl orthotitanate (C$_{16}$H$_{36}$O$_4$Ti, 0.01 mol) was then added and the resulting mixture was stirred for a further 30 min. Meanwhile, 1.5 ml of acetic acid and 1.0 ml of deionized water were added into the mixture. Afterwards, the resulting mixed solution was placed in a Teflon-lined stainless steel autoclave and kept at 120 °C for 20 h. The heated solution was then removed from the oven and allowed to cool to room temperature naturally. The co-doped TiO$_2$ powder [hereafter TOFS] was obtained by filtrating and washing with deionized water and ethanol for several times, and then dried at 80 °C overnight. The resultant TOFS powder was marked as TOFS-120 and then annealed at 350, 450, 600 and 700 °C for 3 h in air to give yellow anatase TOFS. The prepared catalysts were denoted as TOFS-350, TOFS-450, TOFS-600 and TOFS-700, respectively. As a reference, undoped TiO$_2$, F-doped TiO$_2$ [hereafter TOF] and S-doped TiO$_2$ [hereafter TOS] were also synthesized using the same approach with NH$_4$F and CH$_4$N$_2$S as starting materials, respectively.

2.2. Photocatalytic performance testing

Photocatalytic reactions were carried out in an opened reactor under visible light irradiation using a 300 W Xenon lamp (Trusttech, Beijing, China) equipped with 420 nm cut-off glass filter. Various photocatalysts including commercial P25, TOS, TOFS, TOF (150 mg) were added into 150 ml of Methylene Blue (MB, 10 ppm) solution. The suspension was stirred in the dark for 30 min before visible light irradiation to ensure the mixture had reached adsorption equilibrium. 3 ml of the solution was extracted every 30 min, the photocatalyst separated from the solution by a centrifugation method and the Methylene Blue concentration of the remaining transparent liquid tested by UV–vis spectrometer. During the photoreactions, no oxygen was bubbled into the suspension.

2.3. Material characterization

The crystal size and crystalline structure of the prepared doped TiO$_2$ samples were determined by X-ray diffraction (XRD) using a Philips X-PeRT Pro Alpha 1 diffractometer operating with Cu Kα radiation ($\lambda = 1.5406$ Å) at a tube current of 40 mA and a voltage of 45 kV. Data were collected over 2θ values from 20° to 80° at a speed of 1°/min. The strongest TiO$_2$ peak, corresponding to anatase (1 0 1), was selected to evaluate the average crystal size by the Scherrer equation. The X-ray photoelectron spectroscopy (XPS) measurements were carried out using a Perkin-Elmer RBD upgraded PHI-5000C ESCA system with monochromatic Mg Kα excitation and a charge neutralizer. All bonding energies were calibrated to the C 1s peak at 284.8 eV of the surface adventitious carbon. Fourier transform infra-red (FT-IR) spectra were obtained using a Bruker Vertex-70 by diffused reflectance accessory technique. Laser Raman spectra were obtained using a Perkin-Elmer Ramanstation 400F Raman spectrometer. UV–vis diffuse reflectance was recorded by a Perkin Elmer Lambda 750S UV/vis spectrometer. The geometry and morphology of the TOFS particles were observed using a HRTEM (JEOL JEM-3000F) operating at 300 kV. The crystal structure was examined by SAED with a selected area of 200 nm. The electronic paramagnetic resonance (EPR) spectra were recorded on an Bruker X-band EMX spectrometer operating at 100 kHz field modulation and 1 mW microwave power and equipped with a high-sensitivity cavity (ER 4119HS). For the EPR spectra, all the samples were directly loaded in the ESR sample tube without further treatment, spectra were recorded on powder samples under liquid nitrogen atmosphere at 130 K and then at room temperature. The *g* values were determined by reference to a DPPH standard. Computer simulation of the EPR spectrum was obtained using the EasySpin program.

3. Results and discussion

Fig. 1 shows the X-ray diffraction data for the TOFS samples prepared by the low-temperature solvothermal method. The structures of as-prepared TOFS-120 are totally different from the annealed samples, which predominantly indicated an amorphous phase. It can be observed that for all annealing temperatures and
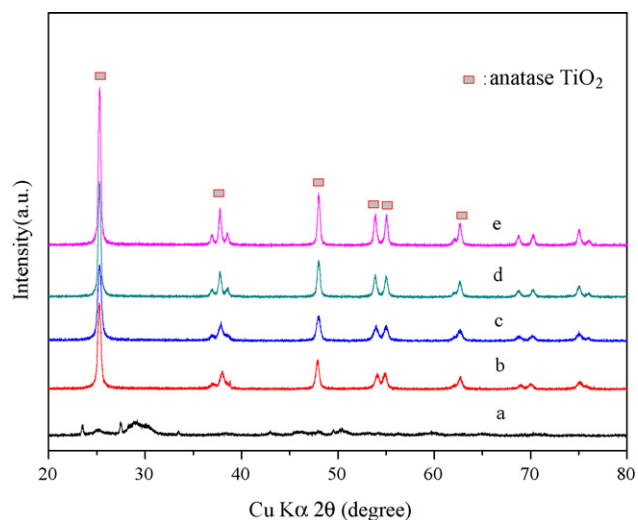
Fig. 1. X-ray diffraction patterns of doped TiO$_2$ samples: (a) TOFS-120; (b) TOFS-350; (c) TOFS-450; (d) TOFS-600; (e) TOFS-700.

for all doping regimes the original TiO_2 nanomaterials transform from an amorphous structure to the anatase phase (JCPDS71-1168) and that there are no significant structural differences between the four annealed F–S co-doped TiO_2 samples. Furthermore, as the calcination temperature increases, the main (1 0 1) Bragg peak anatase is observed to become sharper and more intense, indicative a higher crystalline and larger average crystallite size for the F–S co-doped TiO_2. The crystallite size is thought to increase with calcination temperature because of the agglomeration of particles during high-temperature sintering. Annealing of TOFS-120 at 700 °C significantly increases the particle size of TiO_2. Interestingly, the TOFS-700 sample still possesses the anatase structure even after annealing at 700 °C, which suggests that the F–S co-doped TiO_2 has excellent structural stability at higher temperature and is highly resistant to the phase transformation to rutile. In addition, no characteristic Bragg peaks for F and S titanium compounds were observed in the X-ray diffraction data, indicating that fluorine and sulfur were highly dispersed on TiO_2.

Raman spectroscopy was used to further investigate into the presence of other titanium phases in the F–S co-doped TiO_2 samples annealed at different temperatures. It is well known that laser Raman spectroscopy is a powerful technique that can detect the presence of the additional titanium phases (rutile and brookite) even at very low concentrations. It has been reported that the Raman spectrum of anatase single crystal shows six Raman bands at $144\,cm^{-1}$ (E_g), $197\,cm^{-1}$ (E_g), $399\,cm^{-1}$ (B_{1g}), $513\,cm^{-1}$ (A_{1g}), $519\,cm^{-1}$ (B_{1g}) and $639\,cm^{-1}$ (E_g) [18], and that of the rutile phase displays four Raman bands at $143\,cm^{-1}$ (B_{1g}), $447\,cm^{-1}$ (E_g), $612\,cm^{-1}$ (A_{1g}), and $826\,cm^{-1}$ (B_{2g}) [19]. Fig. 2 presents the Raman spectra of TOFS-350, TOFS-450, TOFS-600 and TOFS-700. It can be observed that the main features of the Raman spectra of all TOFS samples are very similar and that all samples show the characteristic Raman bands of the anatase phase, with no evidence for the corresponding bands of the rutile phase. This finding is in accordance with the result of the X-ray diffraction measurements.

Fig. 3 shows the FT-IR spectra of TOFS-350, TOFS-450, TOFS-550, TOFS-600 and TOFS-700, and undoped TiO_2 (No P25) annealed at 450 °C for 3 h in an air, which can provide more information of functional groups of the catalyst materials. Here, the FT-IR spectra of the TOFS samples annealed at different temperatures exhibit rather similar spectra to titanium oxide, with all the TOFS samples displaying a band at around $700\,cm^{-1}$, which can be attributed to the vibration of Ti–O bond and the Ti–O–Ti bridging stretching modes [20]. The peaks around 1630 and $3400\,cm^{-1}$ correspond to
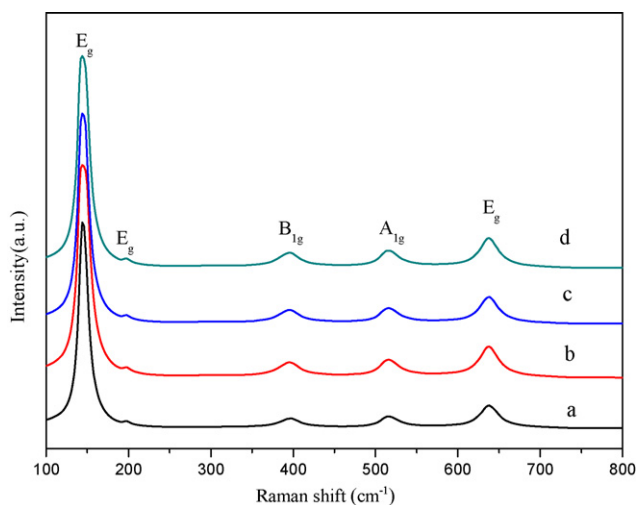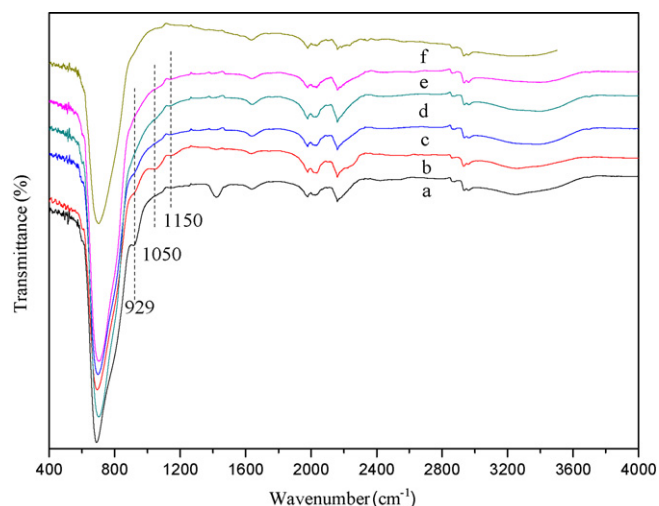
Fig. 3. FT-IR spectra of the TOFS samples: (a) TOFS-350; (b) TOFS-450; (c) TOFS-550; (d) TOFS-600; (e) TOFS-700; (f) undoped TiO_2.

the bending vibrations of the O–H bond and the stretching vibration of –OH or absorbed water molecules, respectively [21–23]. The two peaks located at around 1150 and $1050\,cm^{-1}$ correspond to two distinct S species in the TOFS samples [24]. The FT-IR band at $1150\,cm^{-1}$ corresponds to molecular SO_2 absorbed on the surface of TiO_2 and does not influence the electronic structure of the solid. The other IR band at $1050\,cm^{-1}$, which is of interest, is characteristic of a Ti–S stretching vibration, suggesting the successful doping of sulfur atom into the samples. Another peak may be observed at $929\,cm^{-1}$ in the TOFS-350, TOFS-450 and TOFS-550 samples, and this was ascribed to Ti–F vibrational modes [20,25], which clearly indicates the incorporation of F atom into the TiO_2 lattice. However, no evidence for Ti–F vibration could be found in the TOFS-600 and TOFS-700 samples, indicating that the F–Ti bond is not stable at high temperature. The FT-IR bands related to Ti–F and Ti–S bonds were not found in the pure TiO_2 sample, which suggests that the doping in the various TOFS occurs as a result of the solvothermal process, and does not arise from any impurities present in the precursor TiO_2.

The X-ray photoelectron spectroscopy (XPS) survey spectrum (not shown) indicates that the TOFS sample contains predominantly Ti, O, C, S and F elements, which is consistent with the result of FT-IR spectra (see Fig. 3). The atomic concentrations of the S and F in TOFS-450 sample were found to be 0.8 and 2.1 at.%, respectively. In Fig. 4 we present the F 1s, S 2p Ti 2p and O 1s XPS spectra. Although nitrogen was also introduced into the synthesis system during the sample preparation from the NH_4F and $(NH_2)_2CS$ precursors, no nitrogen was detected in the TOFS surface by XPS, suggesting that nitrogen is not be incorporated into the TOFS under our synthetic conditions.

As shown in Fig. 4, there are two kinds of F states observed in the F 1s XPS spectrum (Fig. 4a). The low binding energy (BE) of around 689.4 eV [14,22] could be ascribed to an F atom substituting for an O atoms, forming a Ti–F bond, while the high BE component located at 696.7 eV is characteristic of an F atom adsorbed to TiO_2 [26]. Similarly, the S 2p XPS spectrum (Fig. 4b) indicates two broad peaks which implied the presence of more than one sulfur species. The asymmetrical S 2p peak (160.7 eV) corresponds to sulfur actually incorporated within the TiO_2 lattice [27], and the higher energy peak (174.8 eV) can be ascribed to surface-adsorbed SO_2 molecules on the TiO_2 surface [28], which may be due to the oxidation of the surface in the annealing process. These results are consistent with those observed by FT-IR spectroscopy.

Fig. 2. Laser Raman spectra of the TOFS samples: (a) TOFS-350; (b) TOFS-450; (c) TOFS-600; (d) TOFS-700.
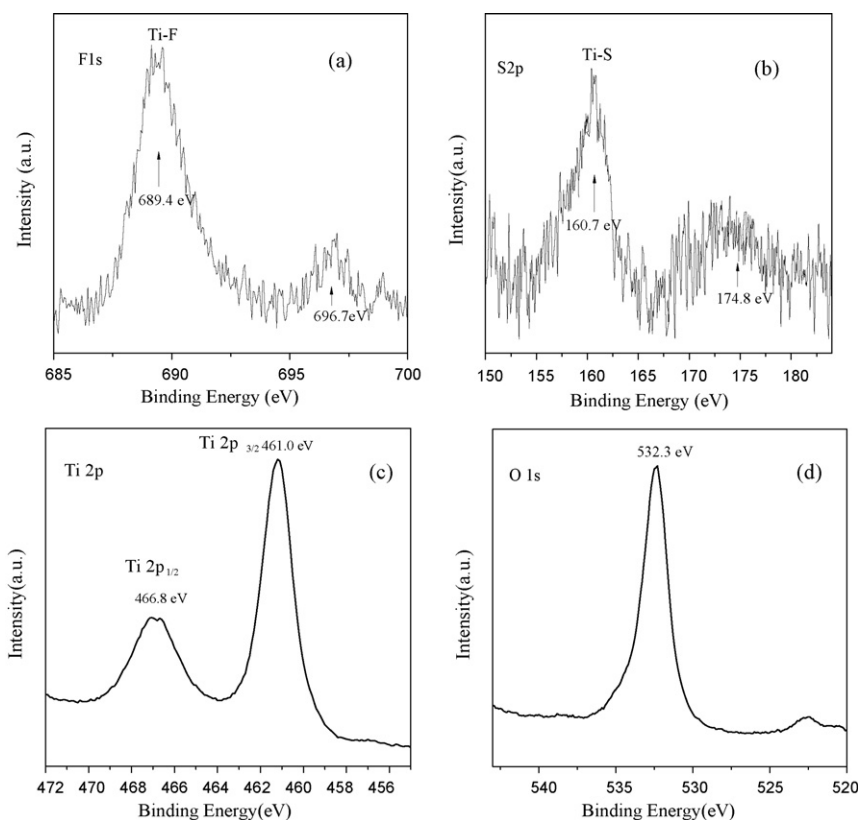
Fig. 4. The XPS spectra of F 1s (a), S 2p (b), Ti 2p (c) and O 1s (d) of F–S co-doped TiO$_2$ sample annealed at 450 °C.

Fig. 4c shows the XPS spectra of Ti 2p in TiO$_2$. It can be seen the binding energy of Ti 2p$_{1/2}$ and Ti 2p$_{3/2}$ was located at 466.8 and 461.0 eV, respectively. In comparison with the Ti 2p binding energy of the annealed TiO$_2$ material and the previously reported literature value [29,30], we found the binding energy of Ti 2p to be 461.0 eV in F–S co-doped TiO$_2$. This increase in binding energy is due to the F and S incorporated in the TiO$_2$ lattice which causes a small structural distortion in the TOFS samples. No evidence for Ti^{3+} was observed in the XPS spectra, although this was observed by EPR (see the result of EPR analysis). The O 1s XPS spectra of F–S co-doped TiO$_2$ annealed at 450 °C is shown in Fig. 4d. It was observed that the O 1s peak around 532.3 eV had shifted by 1.5 eV

in comparison with that of oxygen in pure TiO$_2$ (531.0 ± 0.1 eV). The shifting of O 1s binding energy can be ascribed to doping of the nonmetal species into TiO$_2$.

Fig. 5 shows the HRTEM image and selective area electron diffraction (SAED) of TOFS-450. It can be seen that the co-doped titania presents aggregates of almost rounded nanoparticle morphology, with an average size of 10–15 nm. The phase structure of sample TOFS-450 was also confirmed to be anatase by the SAED analysis.

In order to compare the photocatalytic performance of co-doped TiO$_2$ and mono-nonmetal doped TiO$_2$ under visible light irradiation, the F-only doped TiO$_2$ and S-only doped TiO$_2$ samples were
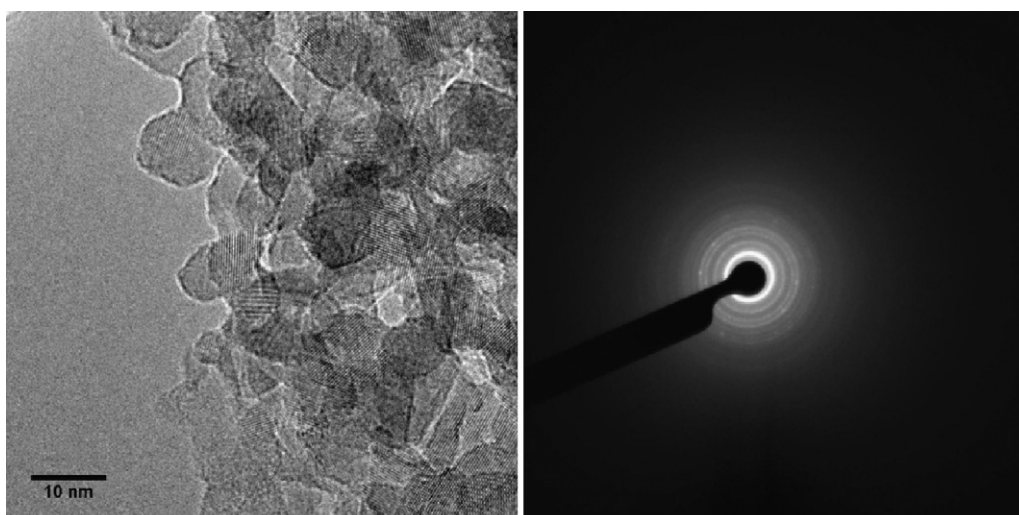
Fig. 5. HRTEM morphology and the SAED image of F–S co-doped TiO$_2$ sample annealed at 450 °C.
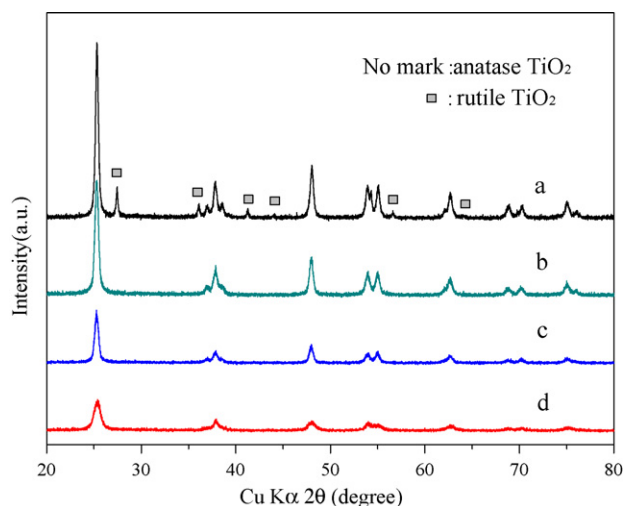
Fig. 6. X-ray diffraction pattern of pure TiO_2 and doped TiO_2 samples: (a) P25 TiO_2 catalyst; (b) TOFS-450; (c) TOS; (d) TOF. All the samples were annealed at 450 °C.

synthesized via the same method and characterized using various techniques. Fig. 6 shows the X-ray diffraction pattern of pure (Degussa P25) TiO_2 and different nonmetal doped TiO_2. All materials have clearly distinguishable crystalline structure. P25, the reference, displays a mixture of rutile and anatase phases with an average crystallite size of 33 nm, whereas TOFS-450 displays only the anatase phase of the doped material, with an average grain size of 15 nm. The average crystal size of TOS (47 nm) and TOF (23 nm) calculated from X-ray diffraction data with the Scherrer equation were clearly bigger than that of TOFS. Interestingly, the photocatalytic activity for both TOS and TOF is poorer than that of the TOFS photocatalyst. This result is in agreement with the reference work [31,32]. Smaller crystallites offer a larger surface area and therefore are expected to exhibit a higher photodegradation activity.

The UV–vis diffuse reflection spectra of pure and doped TiO_2 photocatalyst prepared using the solvothermal method is shown in Fig. 7. Compared with pure TiO_2 (Degussa P25), the doped TiO_2 has a higher absorption in the visible region. The spectra for both TOFS and TOF show two optical absorption edges at 510 and 403 nm, which correspond to band gaps of 2.43 and 3.08 eV, respectively.
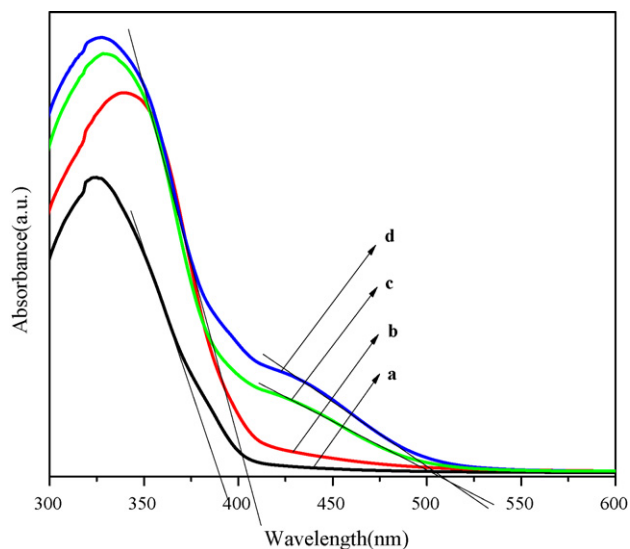
In contrast, the TOS sample shows only one absorption threshold at 405 nm, which corresponds to a band gap of 3.06 eV. The optical absorption of the TOFS sample has a red shift of about 105 nm compared to that of the reference TOS.

A number of studies [33–36] have reported that F-only doping does not lead to a red shift of the absorption edge, as the F atoms form localized levels with high density below the valence band of TiO_2. Therefore, the F 2p state theoretically does not contribute to the visible light absorption of TiO_2. However, it is thought that the observed visible absorption of TOFS and TOF is due to an extremely small amount of nitrogen in the TOFS and TOF samples, even though we could not detect the nitrogen species by XPS analysis (Fig. S1). Additionally, although the absorption intensities and band-edges of TOFS and TOF were quite similar, the TOFS exhibits significant higher photocatalytic activity than that of TOF, which will be discussed later.

The incorporation of the F and S dopants into the TiO_2 lattice is further confirmed by FT-IR spectra. As shown in Fig. 8, all the doped and undoped TiO_2 (Degussa P25) samples calcined at 450 °C show a similar IR absorption. The FT-IR bands around 3400, 1630 and 700 cm^{-1} are indicative of O–H bending and Ti–O stretching. In comparison with the undoped TiO_2, there are some additional bands in the FT-IR spectra of the doped materials. For TOFS-450, we have analyzed (see Fig. 3) these new bands around 929, 1050 and 1150 cm^{-1}, which are ascribed to the vibration of the Ti–F bond, the stretching vibration Ti–S and the adsorption of SO_2 symmetric stretching vibration, respectively. For TOS, the absorbance peaks of Ti–F bond could not be detected, only the characteristic peaks for Ti–S and absorbed SO_2 were observed in the spectrum of TOS. In contrast, TOF only has one additional band at 929 cm^{-1}, which is attributed to the vibration of the Ti–F bond. Based on the above results, we can conclude that the appearance of the Ti–F and Ti–S bonds indicates that F and S atoms were incorporated into the TiO_2 crystal lattice for the TOF and TOS samples.

The photocatalytic performance of the F–S co-doped TiO_2 was tested in an open reactor under a 300 W Xe lamp irradiation equipped with cut-off glass filters. Methylene Blue (MB) was used as the model organic pollutant. The visible light-induced photocatalytic activity for the degradation of Methylene Blue (MB) over F–S co-doped TiO_2 photocatalyst synthesized at different annealed temperatures are shown in Fig. 9. It can be seen that the decomposition curve of P25 photocatalyst is parallel among all the catalyst samples, suggesting that the catalyst has a very weak response to visible light. All the co-doped TiO_2 samples show a higher visi-

Fig. 7. UV–vis absorbance spectra of pure TiO_2 and different nonmetal doped TiO_2: (a) P25 TiO_2 catalyst; (b) TOS; (c) TOFS-450; (d) TOF. All the samples were annealed at 450 °C.
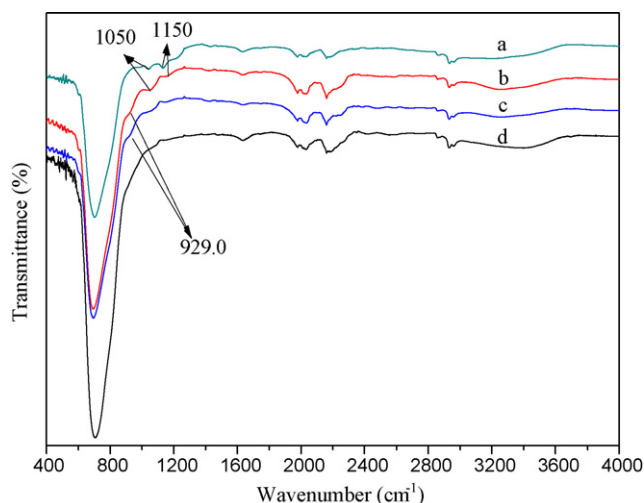
Fig. 8. FT-IR spectra of pure and doped TiO_2 samples: (a) TOS; (b) TOFS-450; (c) TOF; (d) P25 catalyst. All the samples were annealed at 450 °C.
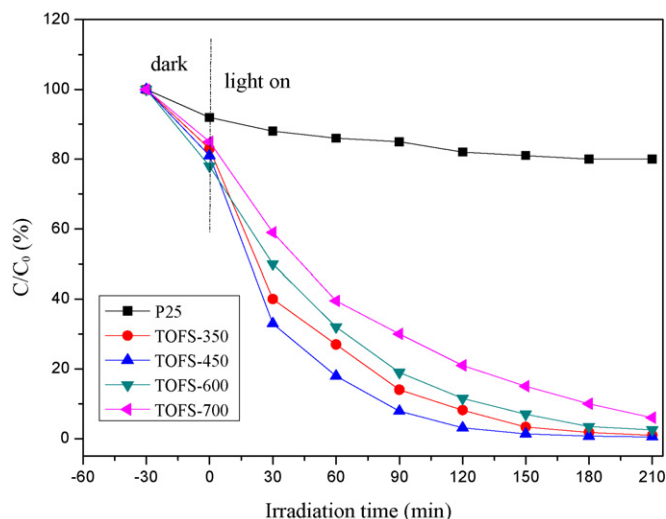
Fig. 9. The photodegradation of Methylene Blue (MB) over different synthesized photocatalysts. Reaction conditions: $C_0 = 10$ ppm and catalyst loading: 1g/L.

ble photocatalytic activity. It also can be seen that the annealing temperature affects the photocatalytic activity, with the TOFS-450 sample showing the highest photodegradation activity with a MB conversion of 97% after 120 min irradiation, which is 5 times higher than that of commercial P25 TiO_2.

To compare the photocatalytic activity of mono-doping and co-doping samples, the photodegradation of Methylene Blue for mono-doping TiO_2 was also investigated under the same conditions. Before photoreaction, the adsorption curve of varying doped samples was performed and the results are shown in Fig. S2. It was found that all of the doped titania samples completely reached adsorption equilibrium within 30 min and the adsorption yield of Methylene Blue solution is 14.3% for TOF, 14.0% for TOFS and 2.5% for TOS, respectively. Fig. 10 shows the visible light-induced photocatalytic decomposition of Methylene Blue (MB) solution with TOFS-450, TOF, and TOS photocatalysts calcined at 450 °C for 3 h. It is worth mentioning here that the visible light photocatalytic activity of F–S co-doped TiO_2 is much higher than that of F-only doping and S-only doped catalysts. Methylene Blue was degraded completely within 150 min, while only 85% of Methylene Blue was degraded over TOF photocatalyst. The TOS show the lowest activ-
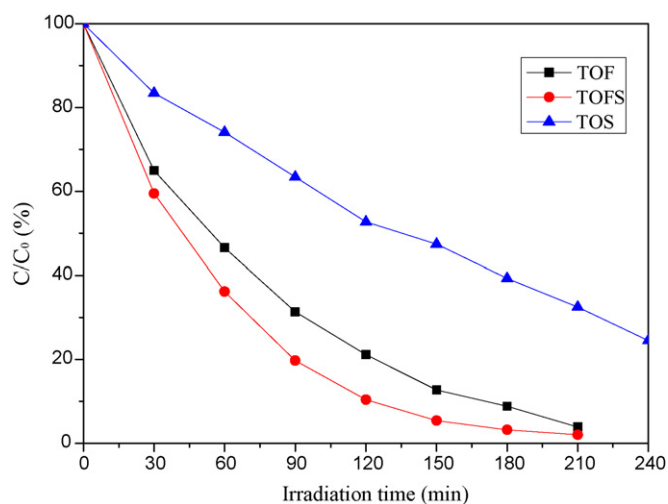
Fig. 10. The photodegradation of Methylene Blue (MB) over different synthesized photocatalysts annealed at 450 °C under visible light irradiation. Reaction conditions: $C_0 = 10$ ppm and catalyst loading: 1 g/l.

ity among the three samples, and the concentration of Methylene Blue solution remains up to 24.5% after 4.0 h irradiation for TOS catalysts. These results suggest that the F–S co-doping of TiO_2 has a synergistic effect for Methylene Blue photocatalytic degradation.

3.1. Mechanisms of visible light-induced photoactivity in F–S co-doped TiO_2

We have also measured the samples using EPR spectroscopy in an attempt to unravel the nature of the defect states and paramagnetic species present in the solid state, with the purpose of better understanding the probable visible light responsive mechanism of co-doped photocatalysts. Fig. 11 shows the experimental EPR spectrum of the doped TiO_2 recorded at varying temperature with the corresponding computer simulation of the spectra, and the parameters used to generate the simulated spectra are given in Table S1. As shown in Fig. 11a, the computer simulation suggests that the spectrum of TOFS is the overlap of two distinct species. The first signal is due to the superoxide radical located on the surface of the oxide sample already observed in the previous work [36,37]. The second signal, at between $g = 1.95$ and $g = 1.99$, is characteristic of bulk and surface Ti^{3+} centers [36–38], the presence of Ti^{3+} ion in the solid is a direct consequence of the inclusion of F in the structure [38], but the Ti^{3+} paramagnetic species is barely observed at room temperature. Similar superoxide and Ti^{3+} ions are also observed in the EPR spectrum of the TOF samples (Fig. 11b).

The experimental and simulated EPR spectra of TOS (Fig. 11c) show a significant difference from those of the TOFS and TOF materials. Here, the signal with a g value of 2.003–1.927 can be confidently assigned to a nitric oxide species [39,40], which was not detected for the TOFS and TOF samples, and it is thought that these species are trapped in closed pores within the crystals or absorbed on the surface, and thus do not influence the electronic structure of the solid. As previously reported [39], the EPR signal of NO could be found at low-temperature ($T < 170$ K), and disappeared at relatively high temperature. To demonstrate this view, the EPR spectra of doped TiO_2 samples were collected at room temperature. As shown in Fig. 11d–f, these spectra are rather similar and the large width of the lines could suggest the presence of either oxygen vacancies or superoxide radical [36,42]. The EPR results presented in this work show that such doping processes can lead to the formation of oxygen anion vacancies [43]. The absorbed oxygen at oxygen vacancy sites was active for the formation of the $O_2^{\bullet-}$ radicals. In addition, the signal of NO was not observed in the EPR spectra of TOS (Fig. 11f), this clearly indicates the NO is a weak adsorbed species, easily desorbed by increasing the temperature. Furthermore, the Ti^{3+} ion was not observed, probably because the relaxation time of Ti^{3+} ions is small enough to cause the broadening of the signal at high temperature [38]. It should be noted that the another N containing species (labeled $N_b^{\bullet}$) which already reported in many studies [38–41] is not observed in the EPR spectra of TOFS and TOF ($N_b^{\bullet}$ can be observed by EPR both at room temperature and at 77 K), indicating the N species does not doped into the TiO_2 lattice by the solvothermal method using the HN_4F and CH_4N_2S as starting materials precursors, although these two chemicals contains many N atoms.

From the above discussion, we tentatively concluded that the F–S co-doped TiO_2 powder produced by the reaction of TiO_2 with thiourea and ammonium fluoride shows visible light photocatalytic activity due to the interaction of the F and S dopants. It should be noted that although the amount of N dopant is extremely low in the TOFS sample, the nitrogen may also have some contribution to the visible light absorption. The S and N atoms incorporated into the TiO_2 lattice may lead to the generation of localized S or N midgap levels, which are located above the O 2p valence band, and narrow the band gap of TiO_2 to induce the shift of optical absorption from
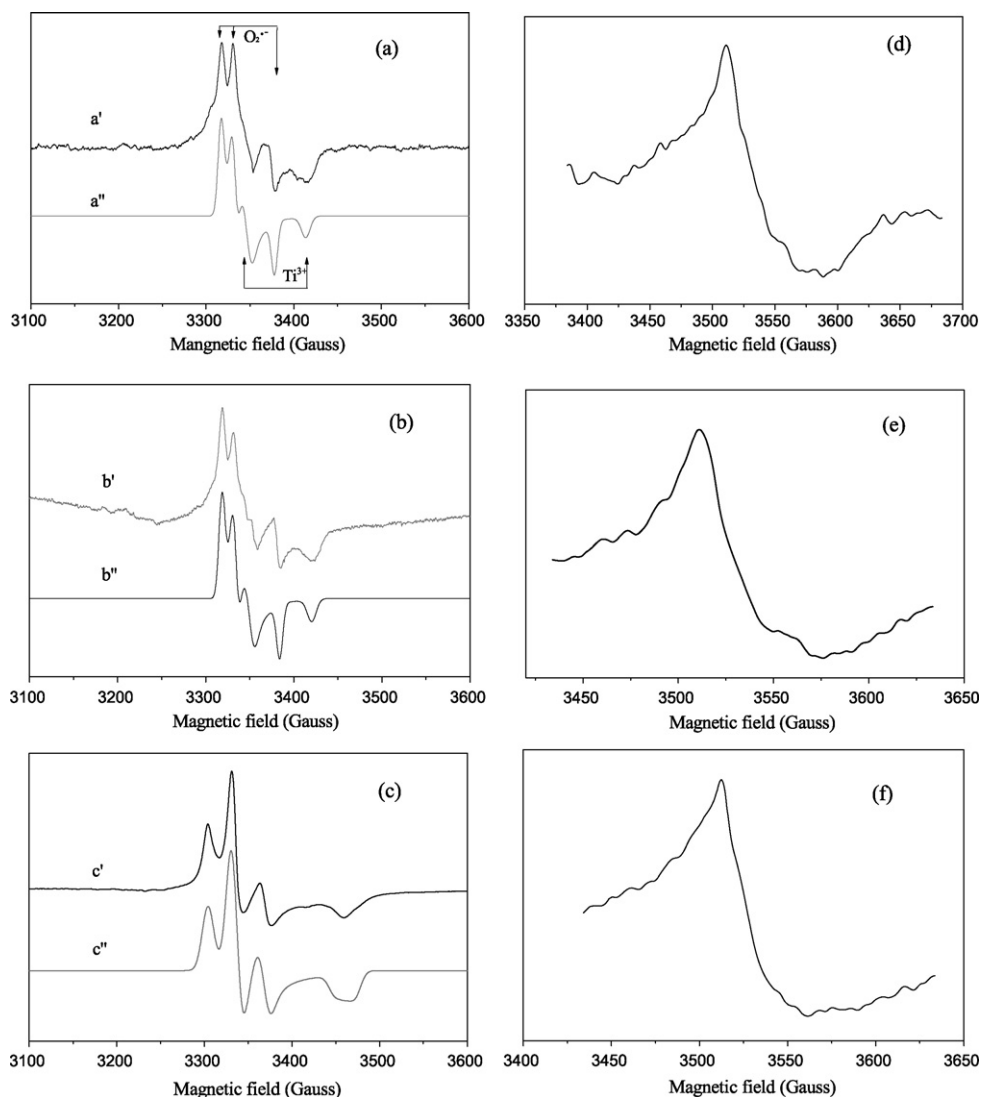
Fig. 11. EPR spectra and corresponding simulation of different synthesized photocatalysts annealed at 450 °C: (a) TOFS-450, (b) TOF, (c) TOS; these three spectra recorded at 130K. (a′, b′ and c′: experimental spectrum; a″, b″ and c″ simulation); (d) TOFS-450, (e) TOF, (f) TOS; recorded at room temperature. Instrument setting: microwave power, 10 dB; microwave frequency, 9.51 GHz; modulation amplitude, 1 G at 100 kHz.

UV region to visible region. Even though fluorine doping does not improve the absorption of visible light, it contributes to the creation of the surface oxygen vacancies, which are important for optical absorption in visible light region. Therefore, it is thought to be the synergic effect of the sulfur or nitrogen impurities, together with oxygen vacancies, that enhances the visible light catalytic activity, while the absorbed F and SO_2 species do not contribute to the observed visible light response of our TOFS system. Furthermore, oxygen vacancies can act as active sites to reduce O_2 and form $O_2^{\bullet-}$ radicals and it is suggested that this superoxide radical is responsible for the decomposition of the organic pollutants, resulting in a increasing decoloration with increasing superoxide species presenting in the catalyst. Moreover, it is believed that because of a synergistic effect between F and S dopants, the co-doped TOFS exhibits the higher photocatalytic activity than observed for mono-doped TiO_2 catalysts.

4. Conclusions

F–S co-doped and mono-doped TiO_2 photocatalyst materials have been prepared using low-temperature solvothermal method,

the resultant materials have been treated under different conditions to give stable doped photocatalysts, which have been characterized by XRD, laser Raman, XPS, FT-IR and EPR and tested for Methylene Blue photocatalytic degradation. The results showed that the solvothermal method can produced doped TiO_2 materials with S and F partially substituted for oxygen, and that this co-doping gives materials with smaller crystallite sizes. The co-doped (F–S) TiO_2 material exhibits higher photocatalytic activity, which is believed due to the synergistic effect between the F and S co-doped into TiO_2 lattice, and the creation of an increased concentration of super oxygen species, thus leading to the enhancement of visible light photoactivities.

Appendix A. Supplementary data

Supplementary data associated with this article can be found, in the online version, at doi:10.1016/j.apcatb.2010.03.004.

References

[1] J.H. Park, T.-W. Lee, M.G. Kang, Chem. Commun. (2008) 2867.
[2] D.V. Bavykin, J.M. Friedrich, F.C. Walsh, Adv. Mater. 18 (2006) 2807.
[3] R. Asahi, T. Morikawa, T. Ohwaki, K. Aoki, Y. Taga, Science 293 (2001) 269–271.
[4] Z. Jiang, F. Yang, N. Luo, B.T.T. Chu, D. Sun, H. Shi, T. Xiao, P.P. Edwards, Chem. Commun. (2008) 6372–6374.
[5] S. In, A. Orlov, F. Garcla, S. Pedrosa-Jimenez, M.S. Tikhov, D.S. Wright, R.M. Lambert, J. Am. Chem. Soc. 129 (2007) 13790–13791.
[6] J. Tang, J.R. Durrant, D.R. Klug, J. Am. Chem. Soc. 130 (2008) 13885–13891.
[7] N. Luo, Z. Jiang, H. Shi, F. Cao, T. Xiao, P.P. Edwards, Int. J. Hydrogen Energy 34 (2009) 125.
[8] J. Zhang, Q. Xu, Z. Feng, M. Li, C. Li, Angew. Chem. Int. Ed. 120 (2008) 1766–1769.
[9] X. Yang, C. Cao, K. Hohn, L. Erickson, R. Maghirang, D. Hamal, K. Klabunde, J. Catal. 252 (2007) 296–302.
[10] X. Yang, C. Salzmann, H. Shi, H. Wang, M.L.H. Green, T. Xiao, J. Phys. Chem. A 112 (2008) 10784–10789.
[11] S.U.M. Khan, M. Al-Shahry, W.B.I. Jr, Science 297 (2002) 2243.
[12] F. Dong, W. Zhao, Z. Wu, Nanotechnology 19 (2008) 1.
[13] D. Chen, Z. Jiang, J. Geng, J. Zhu, D. Yang, J. Nanopart. Res. 11 (2009) 303.
[14] X. Chen, Y. Su, X. Zhang, L. Lei, Chin. Sci. Bull. 53 (2008) 1983–1987.
[15] J.A. Rengifo-Herrera, K. Pierzchala, A. Sienkiewicz, L. Forro, J. Kiwi, C. Pulgarin, Appl. Catal. B 88 (2009) 398–406.
[16] J.H. Xu, J. Li, W.L. Dai, Y. Cao, H. Li, K. Fan, Appl. Catal. B 79 (2008) 72–80.
[17] Y. Su, X. Zhang, M. Zhou, S. Han, L. Lei, J. Photochem. Photobiol. A 194 (2008) 152–160.
[18] K. Yanagisawa, J. Ovenstone, J. Phys. Chem. B 103 (1999) 7781–7787.
[19] K.L. Frindell, M.H. Bartl, A. Popitsch, G.D. Stucky, Angew. Chem. Int. Ed. 41 (2002) 959–962.
[20] D. Huang, S. Liao, S. Quan, L. Liu, Z. He, J. Wan, W. Zhou, J. Mater. Res. 22 (2007) 2389–2397.
[21] X. Chen, X. Wang, Y. Hou, J. Huang, L. Wu, X. Fu, J. Catal. 255 (2008) 59–67.
[22] Y. Huo, Y. Jin, J. Zhu, H. Li, Appl. Catal. B 89 (2009) 543–550.
[23] K.L. Yeung, S.T. Yau, A.J. Maira, J.M. Coronado, J. Soria, P.L. Yue, J. Catal. 219 (2003) 107.
[24] F. Wei, L. Ni, P. Cui, J. Hazard. Mater. 156 (2008) 135–140.
[25] D. Huang, S. Liao, S. Quan, L. Liu, Z. He, J. Wan, W. Zhou, J. Mater. Sci. 42 (2007) 8198.
[26] L. Ley, M. Cardona, Photoemission in Solid II, Springer, Berlin, Heidelberg, 1979.
[27] D. Gonbeau, C. Guimon, G. Pfister-Guillouzo, A. Levasseur, G. Meunier, R. Dormoy, Surf. Sci. 254 (1991) 81.
[28] X. Tang, D. Li, J. Phys. Chem. C 112 (2008) 5407.
[29] Y. Yu, H. Wu, B. Zhu, S. Wang, W. Huang, S. Wu, S. Zhang, Catal. Lett. 121 (2008) 165–171.
[30] M. Drygás, C. Czosnek, R.T. Paine, J.F. Janik, Chem. Mater. 18 (2006) 3122–3129.
[31] H.D. Jang, S.-K. Kim, S.-J. Kim, J. Nanopart. Res. 3 (2001) 141–147.
[32] A.J. Maira, K.L. Yeung, C.Y. Lee, P.L. Yue, C.K. Chan, J. Catal. 192 (2000) 185–196.
[33] K. Mori, K. Maki, S. Kawasaki, S. Yuan, H. Yamashita, Chem. Eng. Sci. 63 (2008) 5069.
[34] J.C. Yu, J. Yu, W. Ho, Z. Jiang, L. Zhang, Chem. Mater. 14 (2002) 3808.
[35] J.K. Zhou, L. Lv, J. Yu, H.L. Li, P.Z. Guo, H. Sun, X.S. Zhao, J. Phys. Chem. C 112 (2008) 5317.
[36] E.A. Reyes-Garcia, Y. Sun, K.R. Reyes-Gil, D. Raftery, Solid State Nucl. Mag. Res. 35 (2009) 78.
[37] J. Soria, J. Sanz, I. Sobrados, J.M. Coronado, F. Fresno, M.D. Hernandez-Alonso, Catal. Today 129 (2007) 240–246.
[38] C. Di Valentin, E. Finazzi, G. Pacchioni, A. Selloni, S. Livraghi, A.M. Czoska, M.C. Paganini, E. Giamello, Chem. Mater. 20 (2008) 3713.
[39] S. Livraghi, M.R. Chierotti, E. Giamello, G. Magnacca, M.C. Paganini, G. Cappelletti, C.L. Bianchi, J. Phys. Chem. C 112 (2008) 17248.
[40] S. Livraghi, A. Votta, M.C. Paganini, E. Giamello, Chem. Commun. 4 (2008) 498–500.
[41] S. Livraghi, M.C. Paganini, E. Giamello, A. Selloni, C. Di Valentin, G. Pacchioni, J. Am. Chem. Soc. 8 (2006) 15670.
[42] S.V. Chong, J. Xia, N. Suresh, K. Yamaki, K. Kadowaki, Solid State Commun. 148 (2008) 345–349.
[43] C. Di Valentin, G. Pacchioni, A. Selloni, S. Livraghi, E. Giamello, J. Phys. Chem. B 109 (2005) 11418.